Dyes and Pigments 95 (2012) 188–193

Contents lists available at SciVerse ScienceDirect

Dyes and Pigments

journal homepage: www.elsevier.com/locate/dyepig

Self assembled TiO_2 with 5-sulfosalicylic acid for improvement its surface properties and photodegradation activity of dye

Shun-Xing Li [a,b,*], Shu-Jie Cai [a], Feng-Ying Zheng [a,b]

[a] Department of Chemistry & Environmental Science, Zhangzhou Normal University, Zhangzhou 363000, PR China
[b] Fujian Province University Key Laboratory of Modern Analytical Science and Separation Technology, Zhangzhou Normal University, Zhangzhou 363000, PR China

ARTICLE INFO

Article history:
Received 6 February 2012
Received in revised form
31 March 2012
Accepted 16 April 2012
Available online 22 April 2012

Keywords:
Nanometer size titanium dioxide
Self assembly
Surface property
Visible light photocatalysis
Adsorption
Dye

ABSTRACT

A new photocatalyst, 5-sulfosalicylic acid grafted TiO_2 (5-SA-TiO_2) was synthesized by a chemical adsorption-based self assembly technique, and its surface properties were characterized by means of XRD, BET, IR, and UV–vis spectra. After self assembly, a stable, yellow complex was formed quickly on TiO_2 surface and then its UV–vis wavelength response range was expanded from 375 nm to 600 nm. The band gap of 5-SA-TiO_2 was 2.95 ev, less than that of TiO_2 (3.10 ev). The crystalline structure of TiO_2 could be adjusted by self assembly, i.e., anatase was transformed into brookite and the proportion between brookite and anatase was increased. After self assembly, the adsorption ratio of acid violet 43 (AV 43) was enhanced from 13.56% to 52.36%, because the crystallite size of both anatase and brookite was smaller, the surface areas were larger, and the affinity of between AV 43 and the catalyst was enhanced for the interactions between phenyl groups. The visible light degradation ratio of TiO_2 was increased by self assembly from 36.60% to 97.01% and 82.65% removal of total organic carbon was achieved.

1. Introduction

More than 10,000 kinds of synthetic dyes are used widely in textile dyeing, paper printing, color photography, and food processing. About 10–15% of these dyes may be found in industrial effluents [1] Among them, anthraquinone dyes are the most resistant to degradation due to their fused aromatic structure, which remain colored for a long time. Moreover, most of these dyes are toxic, carcinogenic, and mutagenic [2] Acid violet 43 is an anthraquinone dye for which it has been noted that it possesses a high chemical/biological oxygen demand [3]. The industrial effluents of this dye are highly toxic to both aquatic and land life forms. It is well known that decolorization of anthraquinone dyes has received much attention, but the photocatalytic degradation of acid violet 43 has not been reported until now.

Photocatalytic oxidation technology was usually adopted for its high efficiency, low energy consumption, simple operation, mild reaction conditions, wide application range, and little secondary pollution [4]. Titanium dioxide is the most widely used photocatalyst for its advantages of large specific surface area, non-toxicity, low cost, and long service life, meanwhile, it may lead to complete mineralization of the pollutants to CO_2, water, and mineral acids [5,6]. However, the use of TiO_2 was limited by its polarity, high surface free energy, and poor dispersing capability. Because of its broad energy gap (Eg = +3.20 ~ 4.50 eV), the photocatalytic process should be induced by the ultraviolet light ($\lambda \leq 387$ nm) [7]. Therefore, in order to improve the photocatalytic activity and to enhance the absorption ability for visible light, many reformative methods for TiO_2 were adopted such as transition-metal doping or implanting (including cobalt [8], platimum [9], and iron [10]), nonmetal doping or coating (including carbon [11], sulfur [12], and nitrogen [13]), surface derivating with arginine [14], tartaric acid [15], isocyanate [16], and combination with gold nanaoparticles [17]. However, the above-mentioned inorganic modified TiO_2 (metal and nonmetal doping TiO_2) can not adequately utilize visible light due to their poor visible absorption; the chemical stabilities of these hybrid photocatalysts are relatively low, the modified molecules are only adsorbed on the TiO_2 surface and no steady chemical bond is formed between TiO_2 and the modified molecules, actually most of the modified layer is easily desorbed or decomposed by a photo irradiation process to result in the decrease of photocatalytic activity during the reaction process. Furthermore, the aforementioned modification methods are time-consuming, costly, and complicated [13].

* Corresponding author. Department of Chemistry & Environmental Science, Zhangzhou Normal University, Xian Qian Zhi Jie 36, Zhangzhou 363000, PR China. Tel.: +86 596 2523251; fax: +86 596 2520035.
E-mail address: lishunxing@fjzs.edu.cn (S.-X. Li).

0143-7208/$ – see front matter © 2012 Elsevier Ltd. All rights reserved.
doi:10.1016/j.dyepig.2012.04.006

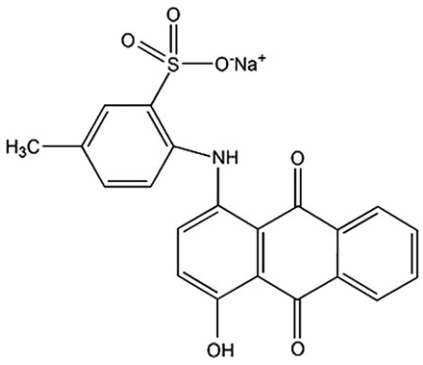

Fig. 1. Molecular structure of Acid violet 43.

To overcome these difficulties, another route to organic modification to TiO_2 is realized by a chemical adsorption through a bidentate six-membered ring interaction between 5-sulfosalicylic acid and −OH groups on the TiO_2 surface. In the present study, acid violet 43 was selected as one typical dye to study the influence of TiO_2 self assembled with 5-sulfosalicylic acid on visible light photocatalytic degradation of organic substances. The photocatalytic degradation factors, including the pH value, the concentration of the catalyst, and irradiation time, were examined. Moreover, obtained titania samples were characterized by means of XRD, BET, IR, and UV–vis spectra. This work may provide new insights and understanding on the mechanisms of photoactivity enhancement by self assembled TiO_2.

2. Experiments

2.1. Materials

Acid violet 43 (AV 43, CAS No. 4430-18-6, its formula shown in the Figs. 1and 2) was purchased from the chemical reagent station in Tokyo, Japan. 5-sulfosalicylic acid (5-SA) was obtained from Sigma chemical Co. (St. Louis, Missouri), its saturated solutions was prepared and used at once, in order to avoid oxidation by dissolved oxygen. All other chemicals were of the highest purity commercially available. De-ionized water used for this study was purified with a Milli-Q water ion-exchange system (Millipore Co., USA) for a resistivity of 18 MΩ cm and used throughout the experiment.

X-ray diffraction (D/max 2400 Rigaku, Japan MAC Science), nitrogen adsorption and desorption experiments (Micromeritics, ASAP 2010, USA), HPLC–MS (Agilent 1200 HPLC and Agilent 6320 ion trap specctrometer equipped with an electrospray ionization source), TOC-V_{CPH} (Shimadzu, Japan), UV–vis scanning spectrophotometer (Perkin Elmer Lambda 900), high-pressure mercury lamp (160 W, Beijing Huate light and Electric Co., China), and PHS-2C pH meter (Mettler-Toledo Delta) were used.

2.2. Preparation of TiO_2 nanoparticles

Nanometer size TiO_2 was prepared by a sol-gel procedure that was used by Su et al. [18]. TiO_2 sols were by the hydrolysis and condensation of titanium (IV) *n*-butoxide in iso-propyl alcohol.

2.3. Self assembly method

Self assembly was carried out through stirring the nano-TiO_2 for 24 h in the saturated solution of 5-SA. After filtered with 0.22 μm membrane filter, the modified TiO_2 was washed with water three times, heat-treated for 30 min at 105 °C. It was worth noting that a yellow coloration developed on the surface of TiO_2, implying that a chemical reaction took place between 5-SA and TiO_2. The catalysts prepared in this way are denoted as 5-SA-TiO_2.

2.4. Characterization of TiO_2 and 5-SA-TiO_2

The crystalline phase and crystal size of TiO_2 and 5-SA-TiO_2 were determined by X-ray diffraction (Cu Kα, 40 kV, 100 mA). XRD patterns were recorded using RINT 2000 goniometer with a secondary graphite monochromator and Cu Kα radiation ($\lambda = 0.15{,}418$ nm). Typical scans were performed in the 2θ 10–80° range, with a sampling range of 0.02°. The crystallite sizes of anatase and brookite were calculated according to the Scherrer equation using the full widths at half-maximum (FWHM) data of each phase [19]. The mass fraction of brookite was calculated according to Eq. ($W_B = 2.721\ A_B/(2.721\ A_B + 0.886A_A)$), Where A_A and A_B represent the integrated intensity of the anatase (101) and brookite (121) peaks, respectively. The Brunauer-Emmett-Teller (BET) surface area and pore size distribution were defined by nitrogen adsorption–desorption experiment. Before measurement the sample was degassed at 350 °C and 10^{-5} mbar for 24 h. UV–vis absorption spectra of samples were obtained for dry pressed disk samples using a UV–vis scan spectrophotometer. Samples were mixed with $BaSO_4$ that does not absorb in the UV–vis radiation range (white standard). Scan range was 200–600 nm. Otherwise, the infrared absorptions were studied adopting IR spectrometer for judging the functional group of TiO_2 and 5-SA-TiO_2. The samples were mixed with potassium bromide and the content of the samples were kept around 1.0%.

2.5. Experimental method

A 250 mL open vessel was used as a photoreactor, into which a certain concentration of AV 43 with a certain pH value and 5-SA-TiO_2 were added. The photoreactor was equipped with an electromagnetic stirrer. The visible radiation was generated by a high-pressure mercury lamp. The photoemission spectrum of mercury lamp was illustrated in Fig. 3.

The visible light intensity was adjusted by changing the distance between the vessel and the lamp. This was detected with an irradiation meter. When the distance was 10 cm, the visible light intensity was 1.24×10^4 lux. The concentration of AV 43 was

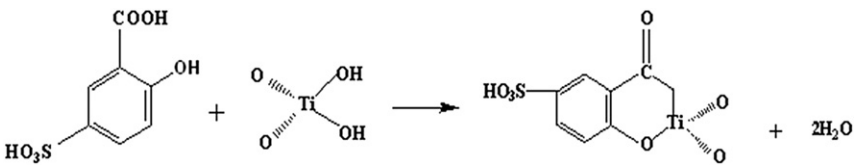

Fig. 2. Chemical adsorption of 5-sulfosalicylic acid onto TiO_2 surface.

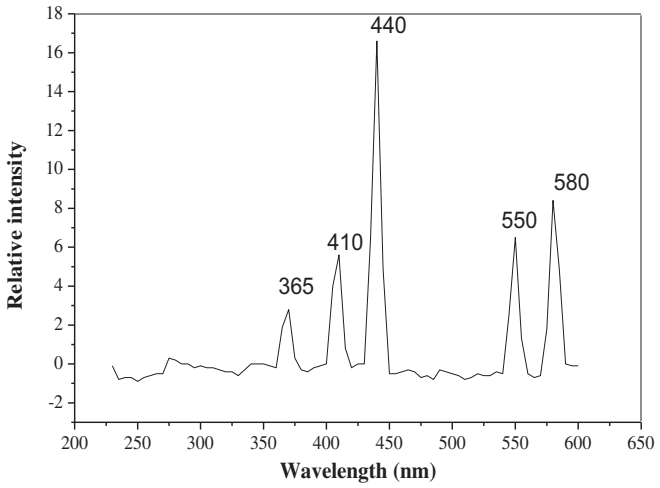

Fig. 3. Emission spectrum of the high-pressure mercury lamp.

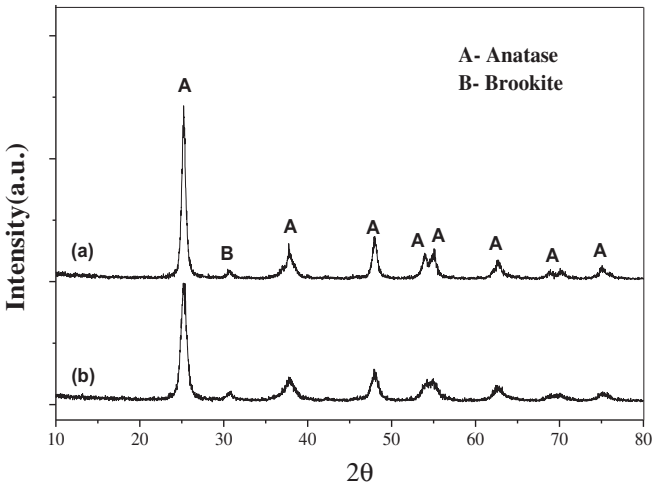

Fig. 4. XRD pattern of samples. (a) TiO_2; (b) 5-SA-TiO_2.

measured by UV–vis spectrophotometer. After being irradiated for a period of time, the aqueous samples were centrifuged at 14,000 rpm to remove catalyst particles from the solution, and then used for the analysis of AV 43 by measuring the absorbance at 560 nm [20].

2.6. Data processing

The photocatalytic degradation ratio was calculated by $(A_0 - A_t)/A_0 \times 100\%$. The A value was proportional to the concentration of AV 43 based on Beer–Lambert law. A_0 was the initial absorbency of the specimen and A_t was the absorbency of the specimen when the photocatalytic degradation time was t.

Using Shimadzu TOC-V_{CPH} model, the total organic carbon (TOC) of the aqueous samples was measured before the irradiation or after irradiation for a certain time (t), the results were denoted as TOC_0 (i.e., initial TOC content) and TOC_t, respectively. The formula, $(TOC_0 - TOC_t)/TOC_0 \times 100\%$, was used for the calculation of the removal of TOC.

3. Results and discussion

3.1. Characterization of TiO_2 and 5-SA-TiO_2

The XRD pattern of the nanoparticles of TiO_2 and 5-SA-TiO_2 is depicted in Fig. 4. The strongest peak at $2\theta = 25.2^\circ$ arose from the (101) anatase phase reflection. Applying the Debye–Scherrer formula to this reflection, the size of crystallites could be estimated. The characteristic small peak at $2\theta = 30.7^\circ$ corresponded to the (121) diffraction peak of brookite phase. The calculated content and the size of brookite crystallites in the samples are reported in Table 1. After self assembly, anatase was transformed into brookite. The activation energy of its transformation was small as 11.9 kJ/mol [21] and it could be offered by the released heat from the chemical adsorption of 5-SA onto TiO_2 surface. So, self assembly was proposed as a post-synthesis treatment method for the adjustment of crystalline structure.

BET surface area and pore volume, together with pore size of TiO_2 and 5-SA-TiO_2 are summarized in Table 1. After self assembly, the BET surface area of TiO_2 was increased from 60.42 m^2/g to 96.46 m^2/g. In Fig. 5, the N_2 adsorption–desorption isotherm and the corresponding pore size distributions calculated by Barrett-Joyner-Halenda (BJH) method were presented. Mainly mesopores were observed on both TiO_2 and 5-SA-TiO_2 with small amounts of micropores, while the hysteresis between the two curves demonstrated that there was a diffusion bottleneck, possibly caused by nonuniform pore size. This pore volume was mainly generated by the interstitial space between adjacent nanoparticles. These pores allowed rapid diffusion of various liquid reactants and products during the photocatalytic reaction. The introduction of 5-SA has led to the increase in the surface area of TiO_2, but its pore size obvious became smaller. It was supposed that 5-SA-TiO_2 had very strong dispersive capacity, which was favorable for photocatalytic reactions.

3.2. Effect of self assembly on wavelength response range and functional group

Fig. 6 illustrates the light absorption properties of TiO_2, 5-SA-TiO_2 and 5-SA. 5-SA did not absorb any light above 400 nm, and TiO_2 absorbed light of wavelengths $\lambda \leq 375$ nm. Following self assembly, the formation of 5-SA-TiO_2 surface complex resulted in a shift of the absorption threshold towards the visible region of the spectrum, up to 600 nm, so the utilization of the light from high-pressure mercury lamp was enhanced. The band energy of 5-SA-TiO_2 surface complex could be estimated from the plots of the square root of Kubelka Munk functions F(R) versus photonenergy [22]. The E_g (band gap energy) value of TiO_2 could be narrowed by the self assembly with 5-SA and its band gap was changed from 3.10 ev to 2.95 ev. The narrower band gap facilitated the excitation of an electron from the valence band to the conduction band, thus the photocatalytic activity of 5-SA-TiO_2 could be increased.

Fig. 7 shows the IR spectra of TiO_2 and 5-SA-TiO_2 samples. The absorption peaks from –OH groups (3182–3213 cm^{-1}, TiO_2 surface), phenyl (1441 and 1477 cm^{-1}), $-SO_3H$ (1167 and 1226 cm^{-1}), and –COOTi– group (1385 cm^{-1}) were observed on 5-SA-TiO_2 surface. TiO_2 nanoparticles possessed a significant number of unsaturated titanium atoms, titanium ions readily form complexes with oxygen atoms from various oxygen-containing ligands. Thus, self assembled TiO_2 was realized by a chemical adsorption through a bidentate six-membered ring interaction between 5-SA and –OH groups on TiO_2 surface, as the Fig. 2 shown. TiO_2 self assembled with 5-SA were to enhance the wettability of TiO_2 powder surface, improve dispersive capacity in polar and non-polar solvent and increase the surface coverage of benzenoid pollutants onto TiO_2 surface through phenyl group interaction.

Table 1
Crystallite size, phase content, BET surface area and pore parameters of TiO_2 and 5-SA-TiO_2.

Sample	Crystallite size[a] (nm)	Phase	Surface area[b] (m^2/g)	Pore volume[c] (cm^3/g)	Pore size[d] (nm)
TiO_2	A(18.89); B(34.66)	A(0.86); B(0.14)	60.42	0.17	11.89
5-SA_TiO_2	A(9.76); B(15.73)	A(0.81); B(0.19)	96.46	0.20	8.44

[a] The anatase and brookite phases were marked with A and B.
[b] BET surface area calculated from the linear part of the BET plot.
[c] Total pore volume, taken from the volume of N_2 adsorbed at about $P/P_0 = 0.97$.
[d] Average pore diameter, estimated using the adsorption branch of the isotherm and the Barrett-Joyner-Halenda (BJH) formula.

3.3. Effect of pH value on the degradation ratio of AV 43

The effect of pH on the degradation ratio of AV 43 was shown in Fig. 8. The degradation ratio was increased with the increase of the pH value from 3.0 to 5.0 but was decreased with the further increase of the pH from 5.0 to 9.0. So, the optimum pH value for the photodegradation of AV 43 was 5.0. The oxidation of organic compounds was first initiated by free radicals (including ·OH) [20]. There were two different reaction pathways for the formation of ·OH. At a high pH value, the ·OH was directly transferred to the active surface of TiO_2 by OH^- and it was produced by capturing photogenerated holes. However, at a low pH value, ·OH was produced through a further reaction on the basis of H_2O_2 formed by the combination of H^+ and the adsorbed O^{2-}. Most studies have confirmed that the latter pathway more easily forms ·OH [20]. Thus the degradation ratio of AV 43 was higher at lower pH than that at higher pH.

In the aqueous solution, the sulphonate groups of the acid dye (D-SO_3Na, including AV 43) were dissociated and converted to anionic dye ions.

$$D - SO_3Na \xrightarrow{+H_2O} D - SO_3^- + Na^+$$

The isoelectric point of TiO_2 was 5.1 [23]. Thus, the TiO_2 surface would remain positively charged in acidic medium (pH < 5.1) and negatively charged in alkaline medium (pH > 5.1). For pH at 5.0, a significantly high electrostatic attraction existed between the positively charged surface of the catalyst and the anionic dye. As the pH of the system increased, the number of negatively charged sites increased and the number of positively charged sites decreased. A negatively charged surface site on the catalyst did not favour the adsorption of dye anions due to electrostatic repulsion. In addition, there was competition between OH^- (at high pH) and D-SO_3^- for positively charged adsorption sites.

3.4. Effect of the catalyst concentration on the degradation ratio of AV 43

The influence of catalyst concentration on the degradation efficiency of AV 43 is shown in Table 2. The photodegradation ratio was increased with the addition of 5-SA-TiO_2 from 0.25 to 1.00 g/L because the active sites for the production of ·OH radicals was increased. However, the degradation ratio of AV 43 declined with the increase in concentration of 5-SA-TiO_2, and it might due to the absorption of light by 5-SA-TiO_2 was obstructed greatly for its interception and scattering of light, and the photocatalytic reaction could not be taken place without light-induction. Another reason might be due to the particle interactive behaviour, such as aggregation, resulted from high catalyst concentration. Such aggregation of 5-SA-TiO_2 nanoparticles would lead to decrease in total surface area available for degradation, reduce the site density for surface holes and electrons, and increase in the diffusion path length [24].

3.5. Effect of the irradiation time on the photodegradation ratio of AV 43

After the photodegradation for 0–40 min, the UV–vis absorption spectral of AV 43 were studied and the results were shown in Fig. 9. The bands relating to different molecular parts in AV 43 and its degradation products were decreased significantly with respect to irradiation time.

The obtained spectra indicated the strong distinctive absorbance peaks at about 282 nm wavelength. The absorbance peaks at around this wavelength were attributed to an aromatic ring absorption [25]. The hydroxyl radicals from light-induced generation could attack to the aromatic rings [26]. After irradiation

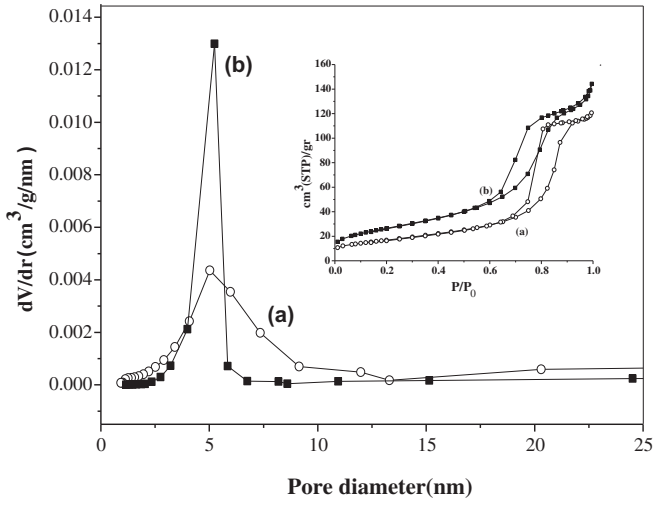

Fig. 5. Pore size distribution curves and the corresponding nitrogen adsorption/desorption isotherms (inset) for samples. (a) TiO_2; (b) 5-SA-TiO_2.

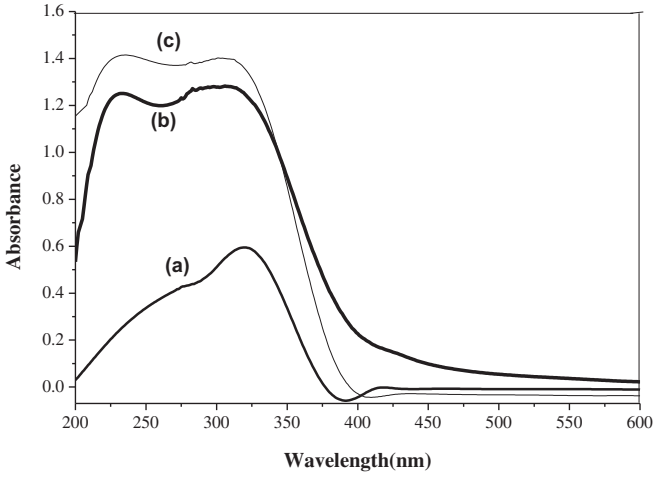

Fig. 6. UV–vis absorption spectra of samples. (a) TiO_2; (b) 5-SA-TiO_2; (c) 5-SA.

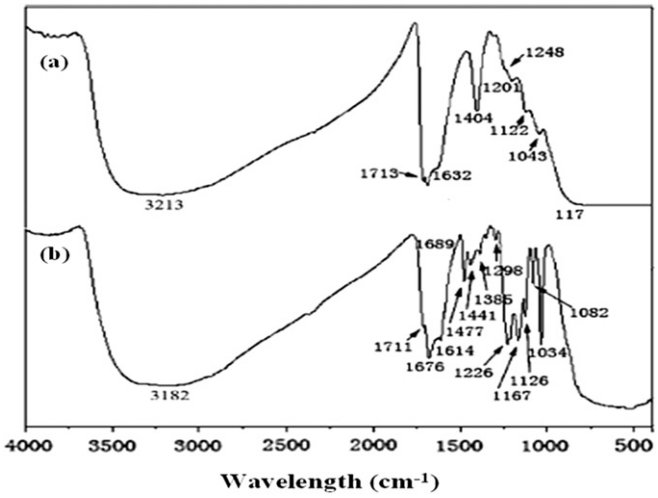

Fig. 7. Infrared spectra of samples. (a) TiO_2; (b) 5-SA-TiO_2.

40 min, a nearly perfect disappearance of the band at 282 nm therefore revealed that the aromatic group of AV 43 was eliminated. The other main absorption peak at approximately 560 nm also decreased continuously with the increase of the irradiation time. The chromophores in AV 43 could be almost completely photodegraded by 5-SA-TiO_2 for irradiation of 40 min duration and these results had been confirmed by HPLC-MS.

3.6. Effect of self assembly on the adsorption and photodegradation of AV 43

The optimal photodegradation conditions were used for the adsorption and photodegradation of AV 43, including initial pH 5.0, acid violet 43 0.1 mmol/L, 5-SA-TiO_2 1 g/L, and irradiation time 40 min with high-pressure mercury lamp. At the same time, a blank experiment, i.e., the absence of 5-SA-TiO_2, was carried out and the removal ratio of AV 43 was only 3.64%.

As shown in Table 3, after self assembly, both the adsorption ability and photodegradation activity were improved 3.86 and 2.65 times, respectively, and these improvements might be due to the self assembly for three reasons.

Table 2
Effect of the *catalyst concentration* on the degradation ratio of AV 43. Experimental conditions: initial concentration of AV 43 (0.1 mmol/L), pH (5.0), irradiation time (40 min).

Catalyst concentration (g/L)	0.25	0.5	0.75	1.00	1.25	1.50	1.75	2.00
Degradation ratio (%)	30.21	57.48	80.36	97.01	90.69	84.73	79.45	70.49

Firstly, the surface properties of TiO_2 were improved, including the proportion between brookite and anatase, the crystallite size of both anatase and brookite, and the surface areas. The photocatalytic activity of TiO_2 nanoparticles depended on several factors including specific surface area, crystallinity, crystallite size and crystal structure [27]. The reduced size of the particles led to larger surface areas, and consequently the number of available surface active sizes increases. A reduction in particle size should also lead to a high photonic efficiency favoring a higher interfacial charge carrier transfer rate. The photocatalytic activity of anatase–brookite composite nanocrystals was greater than that of a single-phase anatase sample with comparable crystallite size and surface area [28], because the band gap of TiO_2 nanoparticles in the mixed phase was lower than that of pure anatase or brookite [28], the junction between anatase and brookite was easily to be overcome [27], and the migration of holes or electrons from one semiconductor to another was allowed whereas recombination of the electron/hole pairs was retarded [28]. Because brookite nanocrystals were more photoactive than anatase for the photodegradation of acetaldehyde [29], 4-chlorophenol [30], and 2-propanol [31], the photocatalytic activity might be improved by the increasing of the proportion between brookite and anatase.

Secondly, the affinity between AV 43 and the catalyst was enhanced for the interactions between phenyl groups, the diffusion rate of AV 43 from the solution to the catalyst surface was increased, and then the photodegradation rate was enhanced.

Thirdly, all of the visible light absorption, the electron-transfer rates, and the formation of mobile OH radicals (not surface-bound OH radicals) could be promoted by the formation of the surface complexes [32].

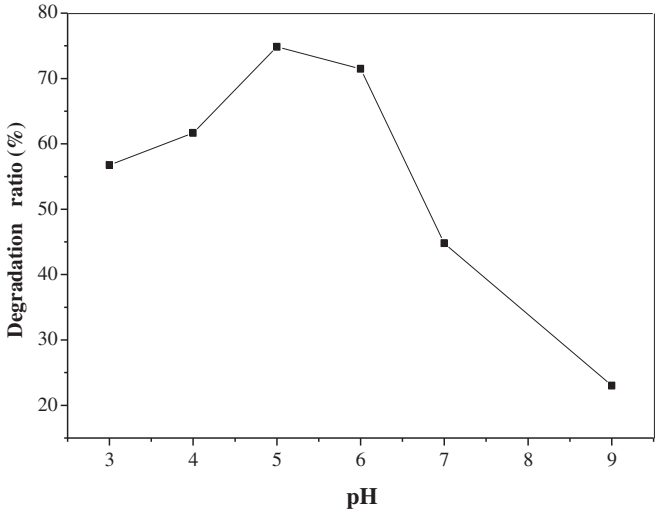

Fig. 8. Effect of pH on the degradation ratio of AV 43. Experimental conditions: initial concentration of AV 43 (0.1 mmol/L), volume (50 mL), catalyst dosage (20 mg), pH (3.0, 4.0, 5.0, 6.0, 7.0, and 9.0), irradiation time (40 min).

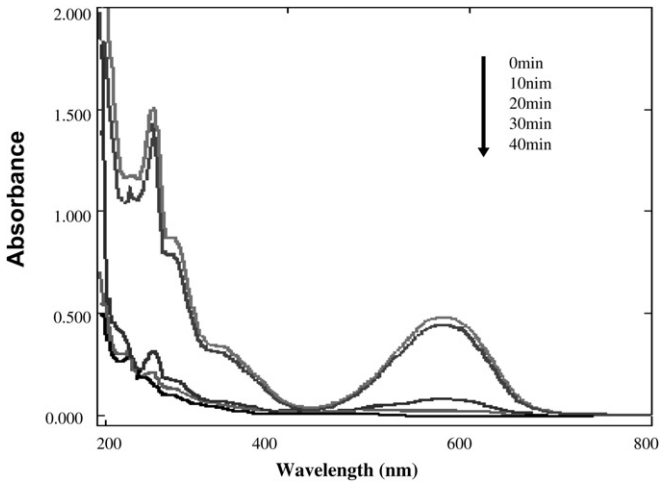

Fig. 9. UV–vis absorption spectral of AV 43 concentration against the 5-SA-TiO_2 under visible light. Experimental conditions: initial concentration of AV 43(0.1 mmol/L), volume(50 mL), catalyst dosage(50 mg), pH (5.0).

Table 3
Effect of self assembly on the adsorption and photodegradation ratio of AV 43. Experimental conditions: initial concentration of AV 43 (0.10 mmol/L), volume (50 mL), catalyst dosage (50 mg), pH (5.0), irradiation time (40 min).

Experimental conditions	Photodegradation		Adsorption		Visible light alone
	TiO_2	5-SA-TiO_2	TiO_2	5-SA-TiO_2	
Removal ratio (%)	36.60	97.01	13.56	52.36	3.64

3.7. Total organic carbon removal

Besides the removal of colour, the reduction of total organic carbon (TOC) was monitored because the TOC values have been related to the total concentration of organics in the solution and the decrease of TOC could reflect the degree of mineralization at the end of the photocatalytic process. Under the optimal conditions, the removal of TOC achieved in 5-SA-TiO_2 method (82.65%) were higher than unmodified TiO_2 method (48.06%), which confirmed the advantage of 5-SA-TiO_2 on the photodegradation of aromatic pollutants.

4. Conclusions

The surface of nanometer size TiO_2 could be simply and fast self-assembled by chemical adsorption in saturated solution of 5-SA. The chemical adsorption as a new method for the adjustment of crystalline structure and crystallite size, i.e., post-synthesis treatment, was proposed for the first time. After self assembly, a stable, yellow complex was formed quickly on TiO_2 surface. The crystalline structure of TiO_2 could be adjusted by self assembly, i.e., anatase was transformed into brookite and the proportion between brookite and anatase was increased. Moreover, the crystallite size of both anatase and brookite was smaller, the reduced size of the crystallite leads to larger surface areas and consequently the number of available surface active sizes increases, and the surface areas were larger. The formation of 5-SA-TiO_2 results in a shift of the absorption threshold, towards the visible region of the spectrum, up to 600 nm, then the utilization of light from high-pressure mercury lamp is enhanced. The introduction of 5-SA improved the affinity between AV 43 and 5-SA-TiO_2.

Above all, TiO_2 self assembled with 5-SA has many characteristics such as convenience, safety, and high efficiency and it could be applied for the photodegradation of aromatic pollutants.

Acknowledgements

This work was supported by the National Natural Science Foundation of China (Nos. 40506020, 20775067, 20977074, and 21175115), the Program for New Century Excellent Talents in University, Outstanding Youth Science Foundation of Fujian Province, China (No. 2010J06005), and the Science & Technology Committee of Fujian Province, China (No. 2008F5063).

References

[1] Liu WX, Chao YP, Yang XQ. Biodecolorization of azo, anthraquinonic and triphenylmethane dyes by white-rot fungi and a laccase-secreting engineered strain. J Ind Microbiol Biotechnol 2004;31:127–32.
[2] Itoh K, Kitade C, Yatome C. A pathway for biodegradation of an anthraquinone dye, C. I. disperse red 15, by a yeast strain pichia anomala. Bull Environ Contam Toxicol 1996;56:413–8.
[3] Zollinger H. Colour chemistry-synthesis, properties and application of organic dyes and pigments. New York: VCH Publishers; 1987.
[4] Chen D, Ray W. Photocatalytic kinetics of phenol and its derivatives over UV irradiated TiO_2. Appl Catal B 1999;23:143–57.
[5] Tryba B, Morawski AW, Inagaki M. Application of TiO_2-mounted activated carbon to the removal of phenol from water. Appl Catal B 2003;41: 427–33.
[6] Grzechulska J, Morawski AW. Photocatalytic labyrinth flow reactor with immobilized P25 TiO_2 bed for removal of phenol from water. Appl Catal B 2003;46:415–9.
[7] Li SX, Zheng FY, Liu XL, Wu F, Deng NS, Yang JH. Photocatalytic degradation of p-nitrophenol on nanometer size titanium dioxide surface modified with 5-sulfosalicylic acid. Chemosphere 2005;61:589–94.
[8] Li J, Liu S, He Y, Wang J. Adsorption and degradation of the cationic dyes over Co doped amorphous mesoporous titania-silica catalyst under UV and visible light irradiation. Microporous Mesoporous Mater 2008;115:416–25.
[9] Huang ML, Xu CF, Wu ZB, Huang YF, Lin JM, Wu JH. Photocatalytic discolorization of methyl orange solution by Pt modified TiO_2 loaded on natural zeolite. Dyes Pigm 2008;77:327–34.
[10] Zhu J, Zheng W, He B, Zhang J, Anpo M. Characterization of Fe-TiO_2 photocatalysts synthesized by hydrothermal method and their photocatalytic reactivity for degradation of XRG dye diluted in water. J Mol Catal A 2004;216: 35–43.
[11] Hamal DB, Klabunde KJ. Synthesis, characterization, and visible light activity of new nanoparticle photocatalysts based on silver, carbon, and sulfur- doped TiO_2. J Colloid Interface Sci 2007;311:514–22.
[12] Zhao W, Ma WH, Chen CC, Zhao JC, Shuai ZG. Efficient degradation of toxic organic pollutants with $Ni_2O_3/TiO_{2-x}B_x$ under visible irradiation. J Am Chem Soc 2004;126:4782–3.
[13] Asahi R, Morikawa T, Ohwaki T, Aoki K, Taga Y. Visible-light photocatalysis in nitrogen-doped titanium oxides. Science 2001;293:269–71.
[14] Ahn WY, Sheeley SA, Rajh T, Cropek DM. Photocatalytic reduction of 4-nitrophenol with arginine-modified titanium dioxide nanoparticles. Appl Catal B 2007;74:103–10.
[15] Wang N, Zhu L, Deng K, She Y, Yu Y, Tang H. Visible light photocatalytic reduction of Cr(VI) on TiO_2 in situ modified with small molecular weight organic acids. Appl Catal B 2010;95:400–7.
[16] Jiang D, Xu Y, Wu D, Sun Y. Isocyanate-modified TiO_2 visible-light-activated photocatalyst. Appl Catal B 2009;88:165–72.
[17] Silva CG, Juárez R, Marino T, Molinari R, García H. Influence of excitation wavelength (UV or visible light) on the photocatalytic activity of titania containing gold nanoparticles for the generation of hydrogen or oxygen from water. J Am Chem Soc 2011;133:595–602.
[18] Su C, Hong BY, Tseng CM. Sol–gel preparation and photocatalysis of titanium dioxide. Catal Today 2004;96:119–26.
[19] Zhang H, Banfied JF. Understanding polymorphic phase transformation behaviour during growth of nanocrystalline aggregates: insights from TiO_2. J Phys Chem B 2000;104:3481–7.
[20] Belessi V, Romanos G, Boukos N, Lambropoulou D, Trapalia C. Removal of reactive red 195 from aqueous solutions by adsorption on the surface of TiO_2 nanoparticles. J Hazard Mater 2009;170:836–44.
[21] Sano T, Negishi N, Koike K, Takeuchi K, Matsuzawa S, Mater J. Preparation of a visble light-responsive photocatalyst from a complex of Ti^{4+} with a nitrogen-containing ligand. J Mater Chem 2004;14:380–4.
[22] Mitsunobu I, Masayoshi H, Hiromi K. Cobalt ion-doped TiO_2 photocatalyst response to visible light. J Colloid Interface Sci 2000;224:202–4.
[23] Ryu DH, Kim SC, Koo SM, Kim DP. Deposition of titania nanoparticles on spherical silica. J Sol-Gel Sci Technol 2003;26:489–93.
[24] Wang XS, Zhou Y, Yiang Y, Sun C. The removal of basic dyes from aqueous solutions using agricultural by-products. J Hazard Mater 2008;157:374–85.
[25] Pavia DL, Lampman CM, Kriz DL. Introduction to spectroscopy: a guide for students. Saunders College Publishing; 2000 [third].
[26] Chiron S, Fernandez-Alba A, Rodriguez A, Garciacalvo E. Pesticide chemical oxidation state of the art. Water Res 2000;34:366–77.
[27] Paola AD, Cufalo GM, Addamo M, Bellardita R, Campostrini M, Ischia R, et al. Photocatalytic activity of nanocrystalline TiO_2 (brookite, rutile and brookite-based) powders prepared by thermohydrolysis of $TiCl_4$ in aqueous chloride solutions. Colloids Surf A 2008;317:366–76.
[28] Ozawa T, Iwasaki M, Tada H, Akita T, Tanaka K, Ito S. Low temperature synthesis of anatase–brookite composite nanocrystals: the junction effect on photocatalytic activity. J Colloid Interface Sci 2005;281:510–3.
[29] Li JG, Tang C, Li D, Haneda H, Ishigaki T. Monodispersed spherical particles of brookite-type TiO_2: synthesis, characterization, and photocatalytic property. J Am Ceram Soc 2004;87:1358–61.
[30] Bakardjieva S, Stengl V, Szatmary L, Subrt J, Lukac J, Murafa N, et al. Transformation of brookitetype TiO_2 nanocrystals to rutile: correlation between microstructure and photoactivity. J Mater Chem 2006;16: 1709–16.
[31] Addamo M, Bellardita M, Paola AD, Palmisano L. Preparation and photoactivity of nanostructured anatase, rutile and brookite TiO_2 thin films. Chem Commun 2006;47:4943–5.
[32] Kim J, Choi W. TiO_2 modified with both phosphate and platinum and its photocatalytic activities. Appl Catal B 2011;106:39–42.